ISSN 0029-3865

CNPq

CBPF – CENTRO BRASILEIRO DE PESQUISAS FÍSICAS

Notas de Física

CBPF-NF-042/93

Transferred Hyperfine Fields in Rare-Earth Substituted YFe_2 and YNi_2

by

D. Guenzburger, R.R. Sobral and A.P. Guimarães

Rio de Janeiro
1993

ISSN 0029-3865

CBPF-NF-042/93

*Transferred Hyperfine Fields in Rare-Earth Substituted YFe_2 and YNi_2**

by

D. Guenzburger, R.R. Sobral and A.P. Guimarães

Centro Brasileiro de Pesquisas Físicas — CBPF/CNPq
Rua Dr. Xavier Sigaud, 150
22290-180 – Rio de Janeiro, RJ – Brasil

*Classification numbers: 75.20E; 76.60

ABSTRACT

In the intermetallic compounds YFe_2 , the magnetic hyperfine field at the Y nucleus, as measured by ^{89}Y NMR spectroscopy, is affected by the substitution of one or more neighbor Y atom by different rare-earth impurities. In order to understand the underlying mechanisms for the transferred hyperfine interaction, we have performed first-principles calculations, within the local spin-density theory, for embedded clusters representing an Y atom and its vicinity in the compounds $Y_{1-x}R_xFe_2$ (R=Gd, Tb, Ho, Tm and Lu) and $Y_{1-x}Gd_xNi_2$. The contact magnetic hyperfine field and the dipolar field were obtained; the resulting total field was found to increase with the spin of the rare-earth impurity. The contact transferred field was found to arise from direct polarization of the s-electrons by the rare-earth spin.

Key-words: Intermetallic compounds; Hyperfine fields; Electronic strucuture.

I. INTRODUCTION

The rare-earths form a large number of intermetallic compounds with the 3d transition elements [1]; they present very interesting magnetic properties, arising from the coexistence of localized and itinerant forms of magnetism. Among these compounds, the cubic Laves phases have attracted a good deal of attention; they allow the systematic study of magnetic properties of different rare-earth ions in the same high symmetry metallic environment. Furthermore, many interesting magnetic effects may be expected from the interactions of f and d moments on the rare earth and d moments on the transition metal ions. Due to the fact that its valence electrons configuration is similar to the lanthanides, Y is included in the group of the rare-earths.

YFe_2 is an intermetallic compound of cubic Laves phase crystal structure (C15), that orders magnetically at 542 K [1]. Each Y atom is placed on a site of high symmetry ($\bar{4}3m$), and is surrounded by four other second-neighbor Y atoms. Previously, it was thought that the Y atoms in this compound were non-magnetic; it has now been established unambiguously, by experimental [2,3] and theoretical [4,5,6] means, that Y carries a small 4d moment of its own, anti-parallel to the Fe 3d moment. The magnetic hyperfine (hf) field at the Y site in YFe_2 has been measured with Nuclear Magnetic Resonance (NMR) of ^{89}Y , yielding a value of -220 kOe (the negative sign meaning a field anti-parallel to the magnetization) [7,8]. On the other hand, YNi_2, with the same crystallographic structure, is known to be non-magnetic [1]. The pseudo-binary compounds of formula $(Y_{1-x}R_x)Fe_2$, where R is a rare-earth, are formed with the same cubic crystal structure, the R atoms

occupying substitutionally the Y sites.

In the $(Y_{1-x}R_x)Fe_2$ compounds, NMR measurements on ^{89}Y have shown a distribution of hf fields corresponding to different configurations of R neighbors; the hf fields in the neighborhood of the rare-earth impurities increase in magnitude, compared to the field in the pure Y compound [9]. This additional, or transferred, hf field, is negative and amounts to a few kOe. Whether the increase in the Y hyperfine field induced by the rare-earth is produced by direct polarization of the conduction electrons, or indirectly by d-d interactions involving the Fe atoms, is not established. The microscopic mechanisms leading to the magnetic behavior of these pseudo-binary compounds can only be investigated by first-principles electronic structure calculations.

We present results of electronic structure calculations for embedded clusters representing rare-earth substituted YFe_2. The lanthanides considered were Gd, Tb, Ho, Tm and Lu, and the number of R atoms in the clusters were chosen as to simulate configurations of low and high local concentrations of neighbors. Furthermore, clusters representing YNi_2 with Gd substituting for Y were also considered; this last compound being non-magnetic when pure, a comparison with the results for Gd-substituted YFe_2 would throw light on the role played by the coupling with the Fe magnetic moments.

The method employed was the first-principles Discrete Variational (DVM) [10,11], in the framework of Density Functional theory and the local spin-density approximation (LSDA). The clusters of atoms representing the solid are embedded in the potential of several layers of external atoms; the Madelung potential is also taken into account. This method has been proven to

be useful in deriving and understanding magnetic and hyperfine properties of quite a number of metals and alloys. Among others, magnetic moments and hyperfine fields of Fe-Ni [12,13] and Fe-Al [14] alloys were investigated, as well as local moments of impurities in s-p [15,16] and transition metals [17,18]. The atomic clusters representation of the solids is adequate, inasmuch as local properties are being investigated. As mentioned earlier, ^{89}Y NMR spectra of $(Y_{1-x}R_x)Fe_2$ discriminates between different configurations of R neighbors of Y [9,19,20]; similar studies on the pseudo-binary compounds $Y(Fe_{1-x}A_x)_2$ (A=Co, Al, Pt) show well-resolved satellite structures of the Y resonance [21]. These results indicate that the Y hyperfine field is strongly affected by the interactions with the nearest magnetic neighbor atoms, being a further indication of the adequacy of the embedded cluster approach.

This paper is organized as follows: in Section II, the theoretical method is briefly described; in Section III, the analysis of the experimental data is described; in Section IV, results of the electronic structure calculations are presented and discussed, as well as calculated values of magnetic moments, spin densities and Y hyperfine fields. The latter are correlated to the experimental data. In Section V we summarize our conclusions.

II. THEORETICAL METHOD

The method employed was the Discrete Variational [10,11] (DVM), based on Density Functional Theory and the local spin-density approximation (see for example [22]). The solids are represented by clusters of atoms, embedded in

the potential of the external atoms in the crystal. The latter is obtained by generating the atomic electronic density at the sites of several shells of atoms external to the cluster, with numerical atomic LSD calculations. The embedding potential is improved by performing self-consistent field (SCF) atomic calculations for the external atoms, with atomic populations similar to those obtained for atoms in the cluster. The Madelung potential of the crystal is included through the method of Ewald; this is important since, as we shall see, the charges obtained on the atoms are quite large. Localization of cluster orbitals due to the Pauli exclusion principle is simulated by truncation of the potential of the external atoms at the core region [23]. In Figs. 1 and 2 are depicted a view of the isolated cluster, and of the cluster embedded in the immediate environment of the crystal. An Y atom is placed at the center of the cluster, since the atom at this position will be better described, being surrounded by two shells of neighbors.

In the DVM method, the one-particle Kohn-Sham equations [24] are solved (in Hartrees):

$$(h_\sigma - \varepsilon_{i\sigma})\phi_{i\sigma} = (-\nabla^2/2 + V_c + V_{xc}^\sigma - \varepsilon_{i\sigma})\phi_{i\sigma} = 0 \qquad (1)$$

where the Coulomb potential V_c includes inter-electronic repulsion and the electron-nuclear attraction; V_{xc}^σ is the exchange-correlation potential and depends on the spin σ. In the present calculation, we have employed V_{xc}^σ as given by von Barth and Hedin [25], which is, as the Coulomb potential, a functional of the electronic density associated with each spin σ:

$$\rho_\sigma(\vec{r}) = \sum_i n_{i\sigma} |\phi_{i\sigma}(\vec{r})|^2 \qquad (2)$$

where $n_{i\sigma}$ is the occupation of spin-orbital $\phi_{i\sigma}$, determined by Fermi-Dirac statistics. In a spin-polarized computation, $\rho_{\uparrow}$ may be different from $\rho_{\downarrow}$. The spin-orbitals of the clusters are linear expansions (LCAO) on a basis of numerical symmetrized atomic orbitals $\{\chi_j^s\}$:

$$\phi_{i\sigma}(\vec{r}) = \sum_j \chi_j^s(\vec{r}) C_i^{\sigma} \quad . \tag{3}$$

The application of the variational method in a discrete grid of points leads to the secular equations:

$$([H] - [E][S])[C] = 0 \tag{4}$$

where [H] is the energy matrix, [C] is the matrix of eigenvectors and [S] the overlap matrix. All the matrix elements are computed numerically in the tridimensional grid of points. Iterations are made until the set $\{\phi_{i\sigma}\}$ is self-consistent with the potential, within a prescribed accuracy. For the present calculations, electronic charges and moments were converged up to ±0.02. To define electronic charges and magnetic moments, the concept of Mulliken populations [26] is adopted, which is based on the coefficients of the LCAO expansion. The magnetic moments on the atoms are defined as the difference between the total Mulliken populations [26] for spin up and spin down.

In the variational expansion of the cluster spin-orbitals $\phi_{i\sigma}$, all atomic orbitals are included for the central Y atom, for which the hyperfine interactions were calculated. For Fe and Ni, only the 3d, 4s and 4p were kept in the variational basis, the others being kept frozen in the core and

orthogonal to the valence. For the other Y atoms and for the Lanthanides, the valence orbitals and the "shallow core" orbitals (4s and 4p for Y, 5s and 5p for R) were included in the variational space. Atomic basis functions were obtained numerically by LSD calculations, and were optimized in further iterations by considering orbital populations as obtained for the clusters. In these calculations, we considered important to include the 4f orbitals of the lanthanides in the valence; this led to problems of convergence, which were circumvented by inducing fractional occupations of the levels near the Fermi level, by a "thermal distribution" sufficiently broad to allow convergence. This procedure led to a small degree of artificial occupation of the minority spin bands placed around the Fermi level.

In the DVM method, a model potential is employed constructed from multipolar expansions of the electronic charge density around each atomic site [27]. This expansion may be carried to any degree of accuracy; for the present compact solids, we considered sufficient to include only spherical terms, such that the electronic density is given by

$$\rho(\vec{r}) \cong \rho^{M}(\vec{r}) = \sum_{n,l,I} d^{I}_{nl} \rho^{I}_{nl}(\vec{r}), \qquad (5)$$

where

$$\rho^{I}_{nl}(\vec{r}) = \sum_{q}{}' \; |R^{q}_{nl}(r_q)|^2 \, Y^{0}_{0}(\hat{r}_q) \; .$$

$\rho(\vec{r})$ is the total electronic density $\rho_\uparrow + \rho_\downarrow$; a similar expansion is made for $\rho_\uparrow - \rho_\downarrow$. ρ^{I}_{nl} are overlapping charge densities centered at each atom q and R^{q}_{nl} are the atomic radial functions of the basis. The prime on the summation

represents a previously defined set of atoms (usually equivalent by symmetry) and I labels a particular set. The coefficients d^{I}_{nl} in Eq. (5) are determined variationally in each cycle by a least-squares error-minimization procedure, with the condition that $\rho^{M}(\vec{r})$ integrates to the total number of electrons in the cluster. Self-consistency is achieved through convergence of the coefficients, since they ultimately determine the cluster potential.

The tridimensional grid employed in the DV method is divided in two regions. In a spherical volume around each nucleus where a more precise numerical integration is needed, a regular grid of points is defined [28]. In the present calculations, this was done for the central Y atom, where the hf field was calculated, and for the rare earth atoms, where higher numerical precision was found to be necessary. In all other regions of space, the grid points are pseudo-random Diophantine [10,11], induced to be more dense near the nuclei.

The hyperfine contact field (or Fermi field) computed at the Y nucleus, on the site (0,0,0) of the cluster, is given by:

$$H_c = \frac{8\pi}{3} g\mu_B 1/2 \; [\rho_{\uparrow}(0) - \rho_{\downarrow}(0)] \qquad (6)$$

where μ_B is the Bohr magneton. The elements of the dipolar hyperfine tensor are given by:

$$\frac{1}{2} g\mu_B \int (\rho_{\uparrow}(\vec{r}) - \rho_{\downarrow}(\vec{r})) \left(\frac{3x_i x_j - r^2 \delta_{ij}}{r^5} \right) d\tau \quad . \qquad (7)$$

The orbital hyperfine field at the Y site was assumed to be small due to quenching of the orbital angular momentum in the metallic environment, and was

neglected. Therefore, the total hyperfine field H_F is given by:

$$H_F \cong H_C + H_D \quad . \qquad (8)$$

III. ANALYSIS OF THE EXPERIMENTAL DATA

The transferred hf fields at the Y site, in the pseudo-binary intermetallic compounds of formula $(Y_{1-x}R_x)Fe_2$ (with x=0.02), were measured by zero-field spin echo NMR of ^{89}Y [20]. The samples of the pseudo-binary compounds were prepared by melting the high purity constituents in an arc furnace, and were studied at 4.2 K.

The hyperfine fields were obtained from the least-squares analysis of the NMR spectra. Each configuration of rare earth second neighbors gives rise to a line in the spectrum, and the corresponding hf fields were obtained. The configurations are identified by their probability of occurrence, at the concentration of the compound examined, assuming a random occupation of the rare-earth sites by the impurities. In the computer fits, the line intensities are taken as proportional to these probabilities. The results reported in the present work were obtained from a configuration characterized by one single R neighbor near the Y probe atom.

IV. THEORETICAL RESULTS AND DISCUSSION

IVa. Electronic Charge Distribution

All the clusters chosen, representing an Y atom and its immediate environment in the crystal, have Y at its center, surrounded by a shell of 12 transition-metal atoms nearest-neighbors (NN) and by 4 Y or R atoms as next-nearest-neighbors (NNN) (see Figs. 1 and 2). In the clusters, the Y atom at the center is best described, since all its chemical bonds are saturated. The pure compounds are thus represented by the clusters $[YFe_{12}Y_4]$ and $[YNi_{12}Y_4]$; the configurations with only one lanthanide atom substituting for Y in the NNN shell is represented by the clusters $[YFe_{12}(RY_3)]$ and $[YNi_{12}(RY_3)]$. The locally R-concentrated configurations are described by the clusters $[YFe_{12}Y_4]$ and $[YNi_{12}Y_4]$. In the case of the Fe compound, several rare-earths were included (R=Gd, Tb, Ho, Tm and Lu), since we were looking for trends among the heavier lanthanides. For the Ni pseudo-binary compounds, only Gd was considered. All the clusters were embedded in the potential of several shells of atoms of the pure crystals. In the latter, each Y atom is surrounded by alternating shells of Fe (or Ni) and Y.

In Table I are given the atomic charges on the clusters representing YFe_2 and derived pseudo-binary compounds. Table II gives the same information for the Ni compounds studied. The valence Mulliken populations (4d, 5s and 5p) for the central Y atom (Y_c) are also displayed on the tables. The total charge on the clusters was determined self-consistently by assuming in each iteration the Y charge as in the central atom (Y_c), taking into account the stoichiometry [29]. For example, the charge on $[YFe_{12}Y_4]$ representing YFe_2 is

-2.0, since (see Table I) the charge on Y_c is +2.0, and there is an excess of two Fe atoms in the cluster. The "shallow core" orbitals 4s and 4p of Y were seen to hybridize to a small extent, and thus their populations were slightly different from those of the free atom.

From Table I it is seen that the charge on Y_c in the compounds is approximately +2.0, as obtained from the Mulliken analysis, which is based on the coefficients of the expansion on the atomic orbitals of the basis. A different kind of charge definition, based on integration within the Wigner-Seitz spheres of each atom, gives smaller values. For example, for YFe_2 we obtained +0.8 for Y_c. In either definition, however, a significant charge transfer from Y to Fe is observed. The small difference found for the charge on the peripheral Y atoms in the cluster (Y_p) is ascribed to a spurious cluster effect, since for these atoms part of the bonds are truncated. The charge on Y_c is seen to remain remarkably constant as the Y_p atoms are substituted for R, even at higher concentrations. The positive charge on R is slightly smaller than that of Y_p (the atoms with which they should be compared) and is quite constant for all the lanthanides considered, except Lu that displays a somewhat more positive charge. These results are consistent with the very similar Pauling electronegativities of the heavier lanthanides (~ 1.20 - 1.25) [30], the exception being Lu with a slightly smaller electronegativity (~ 1.0). When Fe is substituted for Ni, the charge on Y_c becomes somewhat smaller.

In the clusters with one R atom (Table I), there are three types of Fe atoms, at distances 3.05, 4.78 and 6.04 Å from R (see Fig. 3). From Table I it is seen that these Fe atoms have different charges, in particular the atoms at

4.78 Å, that have a much larger negative charge due to an increased 4p population. A part of these differences is an artifact due to the cluster size. A similar charge distribution is obtained for the Ni atoms in $[YNi_{12}(GdY_3)]$ (Table II).

For the R-substituted YFe_2, as well as for the pure compound, the valence configurations of Y_c are very similar. The 4d population is somewhat increased as compared to the free atom ($4d^1 5s^2 5p^0$), and the 5s and 5p orbitals are almost completely depleted, their electrons filling the conduction band which, in the Mulliken analysis, is made up mostly of the 4s and 4p orbitals of Fe. For pure and substituted YNi_2, the results are similar, except that the 4d populations are slightly higher.

IVb. Transferred Hyperfine Fields

The calculated spin magnetic moments for YFe_2 are $-0.19\mu_B$ for Y_c and $1.39\mu_B$ for Fe. For Y_p the moments are slightly smaller, since they are induced by hybridization and for these atoms the bonds are partly truncated. The total moment per formula unit is $2.65\mu_B$. Experimental results point to somewhat higher values: $2.90\mu_B$ for YFe_2 from magnetometry measurements [31] and $-0.67\mu_B$ on Y estimated from polarized neutron diffraction, of which 20 % is believed to be the orbital moment contribution [2]. Theoretical values of the spin moment for Y range from $-0.29\mu_B$ with a Tight Binding calculation [4] to $-0.38\mu_B$ [6] and $-0.43\mu_B$ [32] with the local density LMTO method, and $0.45\ \mu_B$ [32] with the local density ASW (augmented spherical wave) Method [5]. As described in Section II, the fractional electrons distribution utilized to facilitate convergence has the effect of somewhat underestimating magnetic

effects in the clusters, so that our calculated values should be regarded more as trends among the different compounds. The calculated magnetic moment on Y_c is a sum of the 4d moment ($-0.15\mu_B$) and a small contribution from the conduction electrons, with the same sign ($-0.04\mu_B$).

The contact hyperfine field H_c at the Y atom in YFe_2, calculated at Y_c with the use of Eq. 6, is -154kG, also somewhat underestimated as compared to the experimental value -222kG [21]. Therefore, values for the R-substituted compounds will be presented relative to this value. Due to the local tetrahedral symmetry around Y in YFe_2, the dipolar component of the field H_D vanishes. In the Y contact field, contrary to Fe, the valence contribution (5s) is by far the dominant one.

In Fig.4 are plotted the calculated values of H_c (shifted by the values for YFe_2), and H_D at the Y_c site of the clusters $[YFe_{12}(RY_3)]$. The dipolar fields are created at the Y site by the spin-density asymmetry produced by the presence of one rare earth NNN atom. It is seen that the variation of H_D is almost linear with Z; this is not the case with H_c. Although Lu has a zero 4f spin-moment, its effect on the NNN Y atom is not the same as that produced by an Y atom in the same position, resulting in lower hyperfine fields.

In Fig. 5 the values of H_F for the clusters with four NNN substitutions are compared to those with one substitution. The clusters $[YFe_{12}Y_4]$ also present local tetrahedral symmetry around Y_c, consequently the dipolar field vanishes and the only component considered is H_c. For the locally R-concentrated case, the dependence of H_F with Z of the Lanthanide is much more clear-cut than for only one substituent. The trends presented for the two cases in Fig. 5 show clearly that the increase in H_F is not linear in the

number of R substituents, rather reaching a saturation value; this is due in part to the dipolar field, present only in the low symmetry configuration.

In Fig. 6 the calculated values of H_F for the configurations with one R substituent are compared to the experimental values, obtained from measured data with the analysis described in Section III. Although the trends are similar in both cases, the variation is steeper for the calculated values. This discrepancy suggests that the orbital contribution to the hyperfine field at the Y atom may be non-negligible. This hypothesis is plausible since neutron diffraction measurements on YFe_2 indicate the presence of an orbital moment on Y [2]. Orbital hyperfine fields are usually positive and their inclusion in the calculation would probably decrease the absolute values of the fields; they may also be sensitive to the R substituents. Calculation of orbital fields, however, are beyond the scope of this work.

The variations observed in the Y hyperfine fields along the series of lanthanides are clearly related to the different spin magnetic moments of R. The average transferred hf field in concentrated metallic systems has been observed to be broadly proportional to the spin of R in the compounds RFe_2 and R_2Fe_{17} [1,33] and in R_xHo_{1-x} binary alloys [34]. The local hf field near a rare earth impurity is also expected to be roughly proportional to the spin of the rare earth [34]. Accordingly, one may expect a decrease of the magnitude of the hyperfine field at the Y site, as the rare-earth NNN is varied from Gd to Y or Lu. The mechanism through which this takes place is not obvious. Magnetic polarization in metals is thought to propagate by the mediation of the conduction electrons (RKKY mechanism) [1] or by direct, localized d-d hybridization [35]. The situation here is even more complex, since we are

dealing with the influence of R on second-neighbor atoms.

First-principles band-structure calculations for YFe_2 have shown that the observed pressure dependence of the Y hf field is due to the fact that this field originates from the polarization of the s conduction electrons by the Fe(3d) magnetic moments [36]. In the case of the lanthanides, the 4f spin moments polarize the 5d electrons [34]; these in turn may hybridize with the d electrons of Fe and Y. One question which poses itself is whether the transferred hf fields H_c on Y originate from increased 4d magnetic moments on Y, or from direct polarization of the s cloud by the R 4f and 5d electrons. To answer this question, we have plotted in Fig. 7 the 5d spin magnetic moments of the rare-earths investigated, together with the Y_c magnetic moments, calculated for the clusters $[YFe_{12}(RY_3)]$. In Fig. 7, the R 5d moments are divided by $\mu(4d)$ of Y_p in YFe_2 and the Y 4d moments are divided by $\mu(4d)$ of Y_c in YFe_2. It is seen from the figure that $\mu(5d)$ varies significantly with Z of the lanthanide, and thus with the 4f moments of R (calculated $\mu(4f)$ are slightly lower than the free atom values, due mainly to some intra-atomic 5d→4f charge transfer which occurs mainly into the minority spin 4f levels; the values are Gd $4f^{-6.4}$, Tb $4f^{-5.3}$, Ho $4f^{-3.1}$, Tm $4f^{-0.4}$). The Y magnetic moments, however, remain almost constant along the series. Therefore, we may conclude that variations in H_c at Y due to different R substituents are not due to changes in $\mu(4d)$ on the Y, but to direct polarization of the conduction electrons by the 4f and 5d electrons of R. The negligible changes in $\mu(4d)$ of Y are readily understood when one realizes that d-d interactions are short-range, while R and Y are second-neighbors.

In Fig. 7, it is seen that $Y_{1-x}Lu_xFe_2$ does not follow the trend of the

other rare-earth substituted compounds, presenting an increased $\mu(5d)$ with respect to $Y_{1-x}Tm_xFe_2$. This is seen to result from intra-atomic 5d → 4f charge transfer: since this cannot take place in Lu, due to the completely filled 4f shell, the 5d population is increased (for both spins), and consequently, so is $\mu(5d)$.

The spin polarization produced by R is also extended to the Fe atoms. This is observed in Fig. 8, where the valence spin density $[\rho_{\uparrow}(\vec{r}) - \rho_{\downarrow}(\vec{r})]$ is plotted in the Fe-Y_c direction for YFe_2 and $Y_{1-x}Gd_xFe_2$ with one and four NNN Gd atoms.

Further insight on the origin of the hf fields is gained by analyzing pure and R-substituted YNi_2. YNi_2 is known to be non-magnetic [1]; indeed, a self-consistent calculation initiated with a rather large magnetic moment on Ni converges fully to the non-magnetic solution. In this case, therefore, the influence of R may be seen without the additional complication of the transition metal magnetism. In Table III are shown results for Gd-substituted YNi_2. It is seen that, although the spin magnetic moment on Y is negligible, non-negligible values of H_D and H_c are obtained on Y. The values found are similar to differences in H_D and H_c values between YFe_2 and $Y_{1-x}Gd_xFe_2$, showing that in the latter roughly the same polarization is superposed to that induced by Fe. Another interesting feature is the 37% reduction of $\mu(5d)$ of Gd in $[YNi_{12}(GdY_3)]$, relative to $\mu(5d)$ of Gd in $[YFe_{12}(GdY_3)]$, showing that the 3d moment of Fe also contributes to polarize the 5d orbital of Gd.

In Figs. 9 and 10 is displayed the valence spin density in $[YNi_{12}(GdY_3)]$, in the Ni - Y_c and Gd - Ni directions, respectively. The polarization induced by Gd extends over Y and Ni; in the latter, we may also see an induced

polarization of the 3d orbital, which is larger in the Gd - Ni direction. In Fi. 11, the spin density for the Gd-concentrated configuration is shown in the Ni - Y_c direction, substantially increased with respect to the dilute case. Finally, in Figs. 12 and 13 we plot the spin density around the Y_c site, in both the Y_c-Gd and Y_c-Y_p directions, for the configurations with one rare-earth NNN neighbor in the $Y_{1-x}R_xNi_2$ and $Y_{1-x}R_xFe_2$ respectively. The asymmetry in $[\rho_{\uparrow}(\vec{r}) - \rho_{\downarrow}(\vec{r})]$ around Y_c is clearly related to the dipolar field H_p.

V. CONCLUSIONS

Through self-consistent local-spin-density calculations for clusters representing an Y atom and its vicinity in $Y_{1-x}R_xFe_2$ and $Y_{1-x}R_xNi_2$, we have gained understanding on the mechanisms related to transferred hyperfine fields. The dipolar hf field is seen to increase significantly in the series Y, Lu → Gd; the variation obtained is almost linear. The contact field at the Y site is seen to originate from direct polarization of the conduction electrons by the 4f and 5d electrons on the rare-earth, and not from increased μ(4d) on Y. The discrepancies found between the calculated and experimental trends in H_F for the configuration with one rare-earth NNN in $Y_{1-x}R_xFe_2$ are suggested to originate from non-negligible orbital hyperfine fields on Y.

ACKNOWLEDGEMENTS

The authors are grateful to Rio Data Centro, the computing center of the Catholic University of Rio de Janeiro, for giving access to their IBM 9121 computer, where these calculations were performed. Thanks are also due to A.A. Gomes for several fruitful discussions.

FIGURE CAPTIONS

Figure 1. Cluster representing Laves phase compounds, centered on Y.

Figure 2. View of cluster surrounded by neighbor atoms in the crystal.

Figure 3. Fe neighbors of R atom in the clusters [$YFe_{12}(RY_3)$].

Figure 4. Components of the hyperfine field at the central Y atom in mono-substituted clusters [$YFe_{12}(RY_3)$] representing $Y_{1-x}R_xFe_2$, relative to YFe_2. (▫) Dipolar field H_D. (●) Fermi or contact field H_c. Lines drawn are to guide the eye.

Figure 5. Sum of the dipolar and contact fields ($H_F=H_D+H_C$) at central Y atom in clusters representing $Y_{1-x}R_xFe_2$, relative to YFe_2. (●) One NNN substitution ([$YFe_{12}(RY_3)$]). (▫) Four NNN substitutions ([$YFe_{12}R_4$]). Lines drawn are to guide the eye.

Figure 6. Experimental (▫) and calculated (●) hyperfine fields at the Y site in compounds $Y_{1-x}R_xFe_2$ with one NNN substitution, relative to YFe_2. Calculated values ($H_F=H_D+H_C$) were obtained at Y_c for clusters [$YFe_{12}(RY_3)$]. Lines drawn are to guide the eye.

Figure 7. Ratios of calculated magnetic moments for [$YFe_{12}(RY_3)$] clusters, representing $Y_{1-x}R_xFe_2$ compounds with one NNN substitution. Lines drawn are to guide the eye.

Figure 8. Valence spin density along the Fe-Y_c direction for [$YFe_{12}Y_4$], [$YFe_{12}(GdY_3)$] and [$YFe_{12}Gd_4$]. In the case of [$YFe_{12}(GdY_3)$], the Fe atom is NN to Gd. For Y, 4s and 4p orbitals are also included.

Figure 9. Valence spin density along the Ni-Y_c direction for [$YNi_{12}(GdY_3)$]. The Ni atom is NN to Gd.

Figure 10. Valence spin density along the Gd-Ni direction for [$YNi_{12}(GdY_3)$].

Figure 11. Valence spin density along the Ni-Y_c direction for [$YNi_{12}Gd_4$].

Figure 12. Valence spin density around Y_c in [$YNi_{12}(GdY_3)$].

Figure 13. Valence spin density around Y_c in [$YFe_{12}(GdY_3)$].

TABLE CAPTIONS

Table I.

Charges and Mulliken populations in clusters representing YFe_2 and $Y_{1-x}R_xFe_2$.

Table II.

Charges and Mulliken populations in clusters representing YNi_2 and $Y_{1-x}Gd_xNi_2$.

Table III.

Magnetic moments and hyperfine fields in clusters representing Gd-substituted YNi_2.

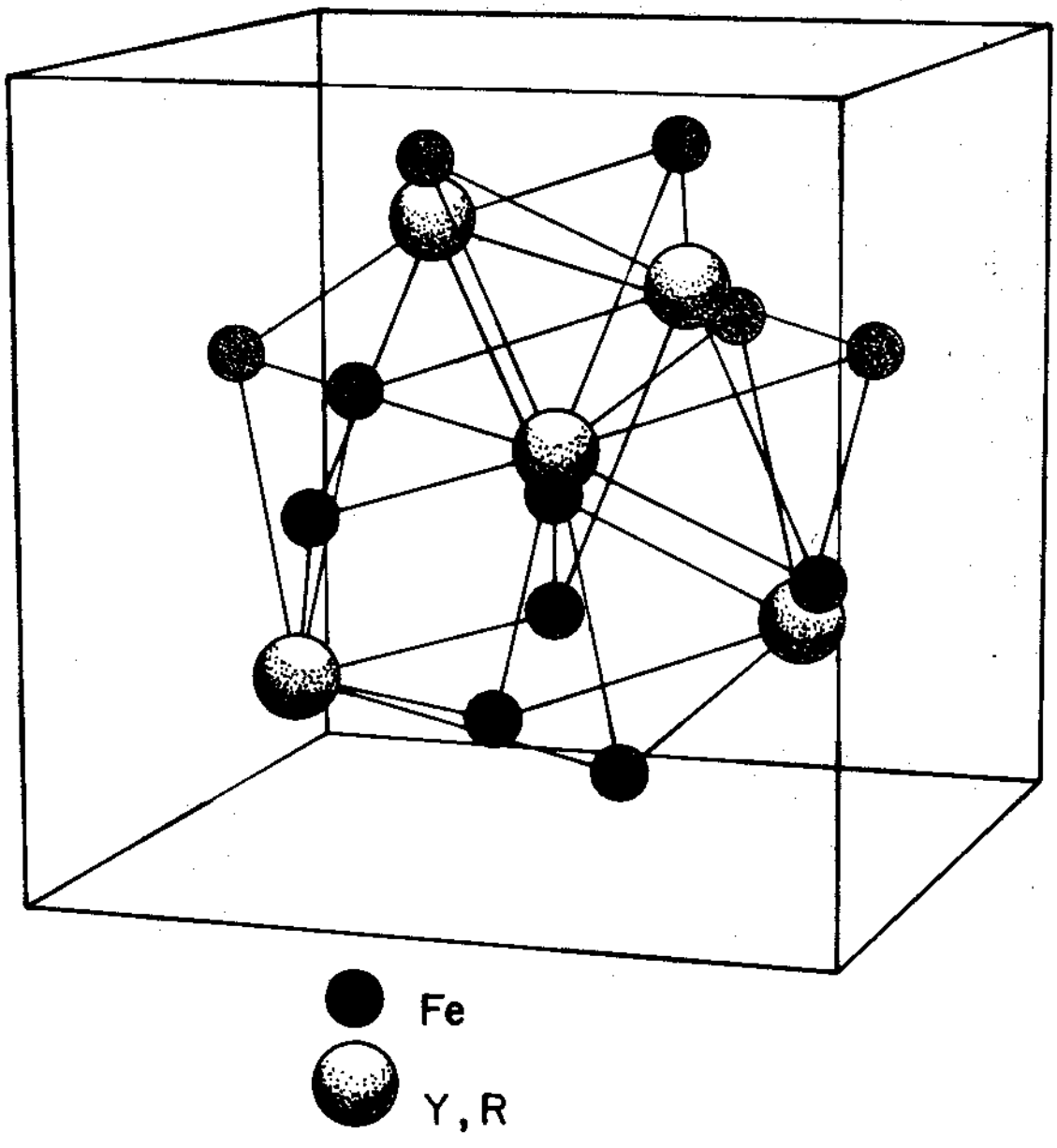

Fig. 1

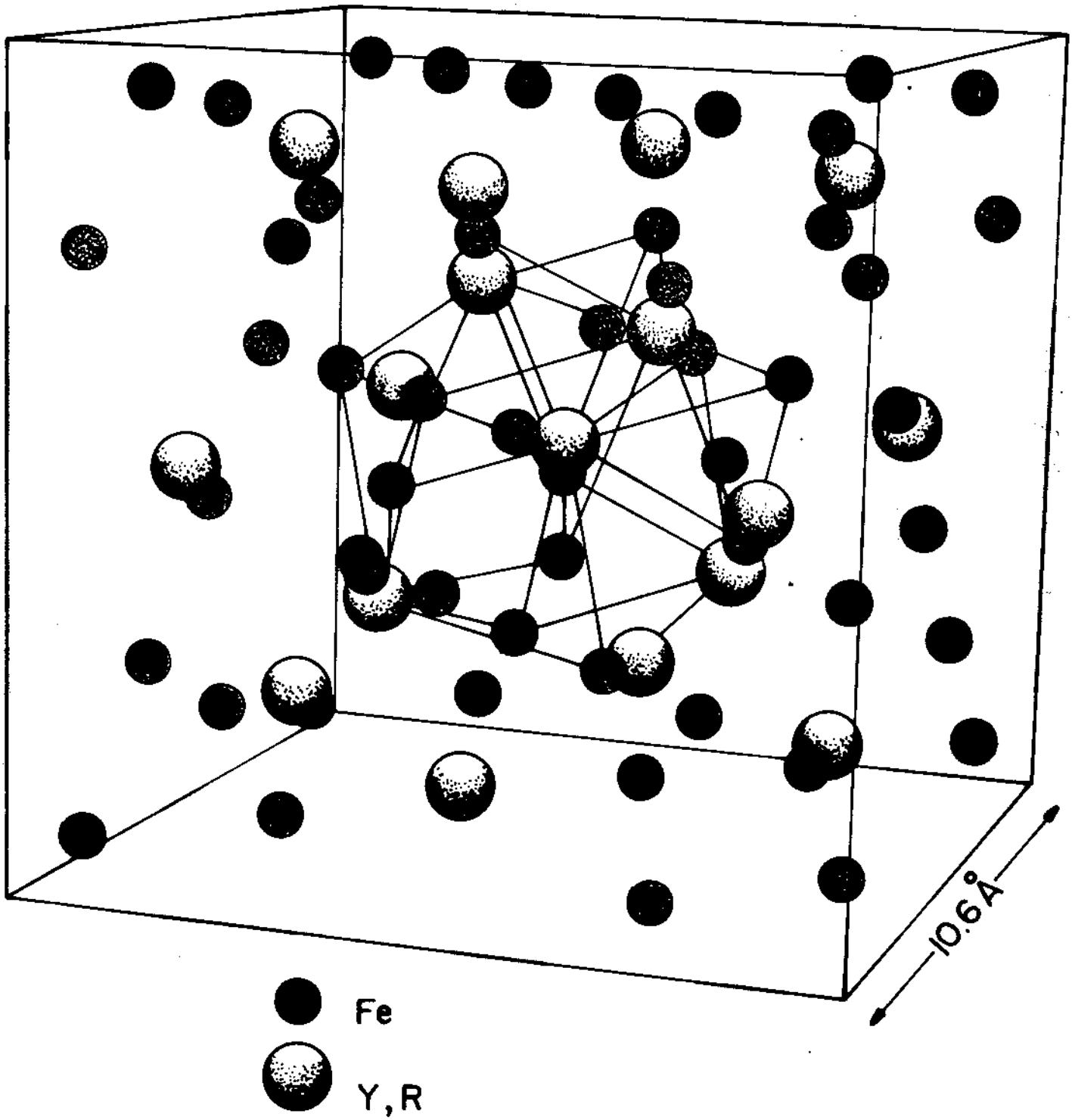

Fig. 2

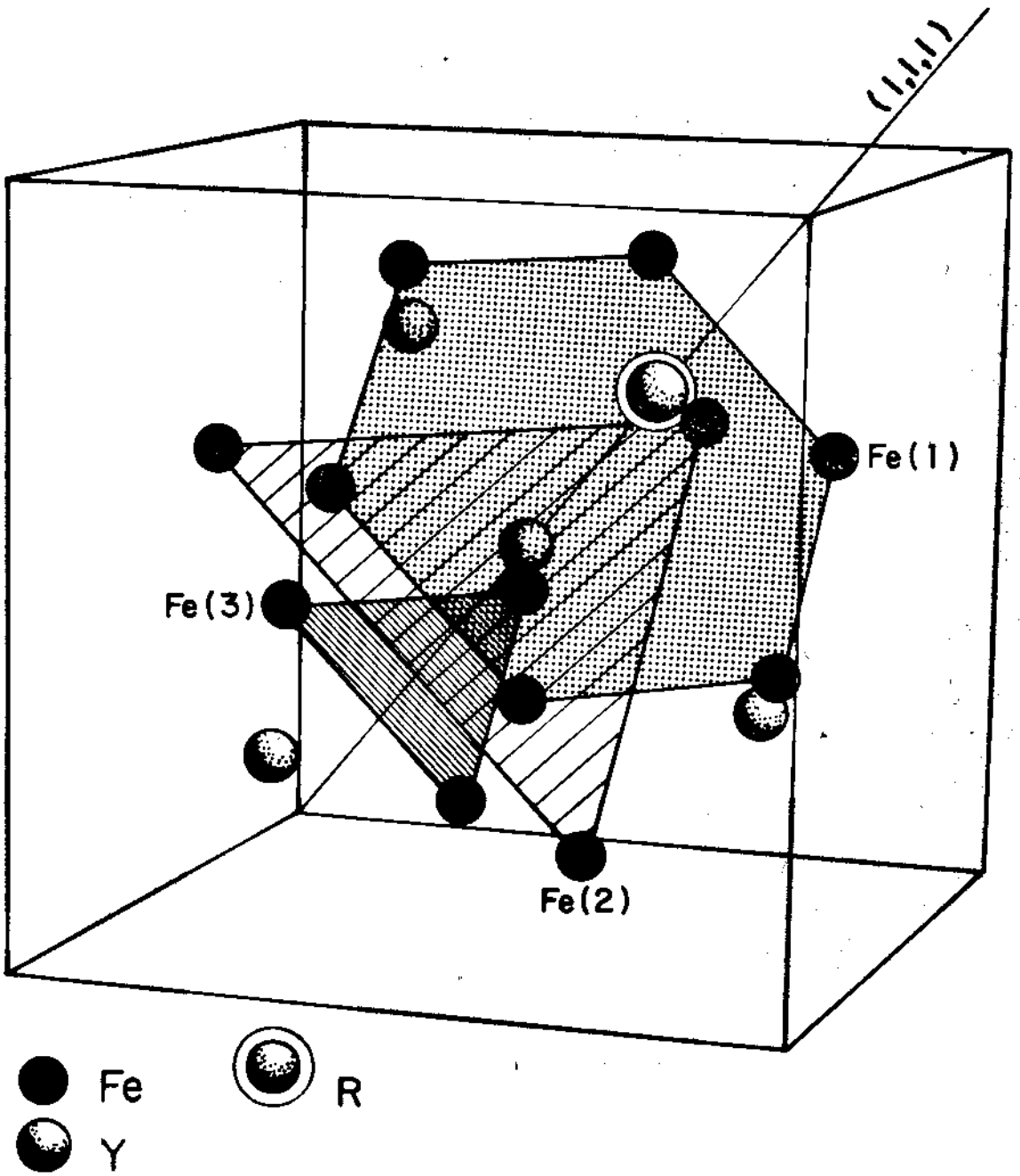

FIG. 3

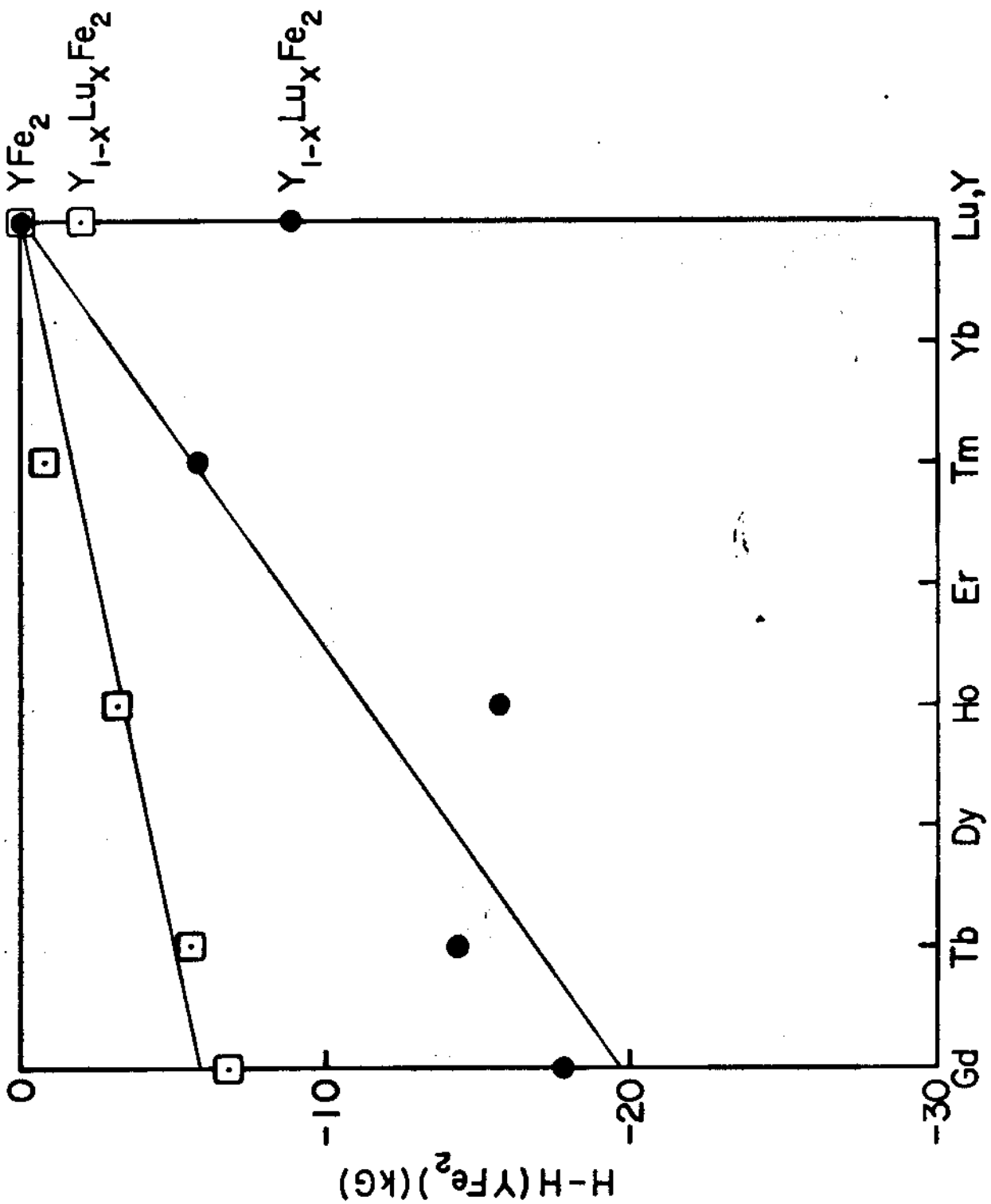
YFe2
Y1-xLuxFe2
Y1-xLuxFe2
0
-10
-20
-30
H-H(YFe2)(kG)
Gd
Tb
Dy
Ho
Er
Tm
Yb
Lu,Y

Fig. 4

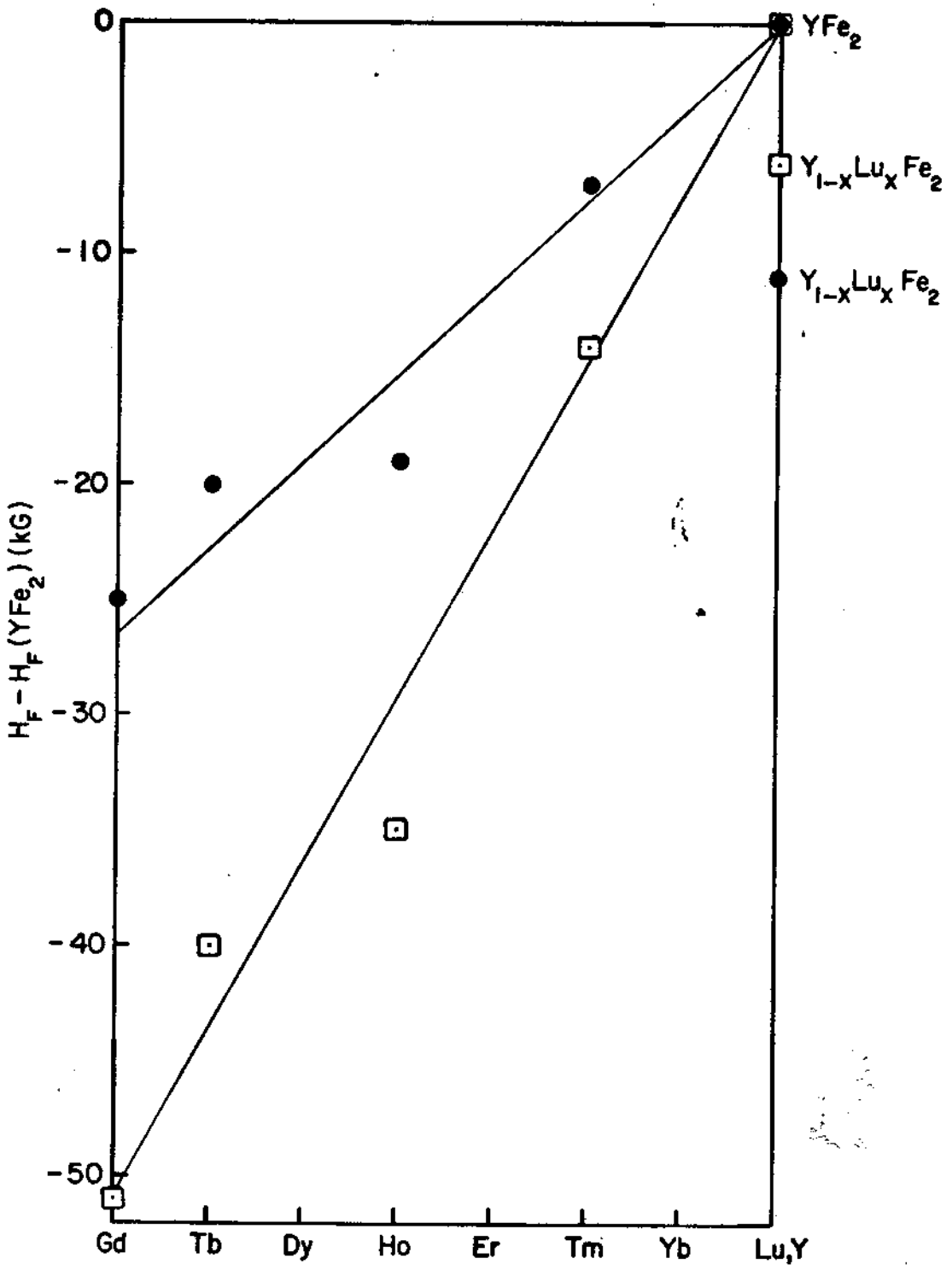
0
-10
-20
-30
-40
-50
$H_F - H_F(YFe_2)$ (kG)
YFe_2
$Y_{1-x}Lu_xFe_2$
$Y_{1-x}Lu_xFe_2$
Gd
Tb
Dy
Ho
Er
Tm
Yb
Lu,Y

Fig. 8

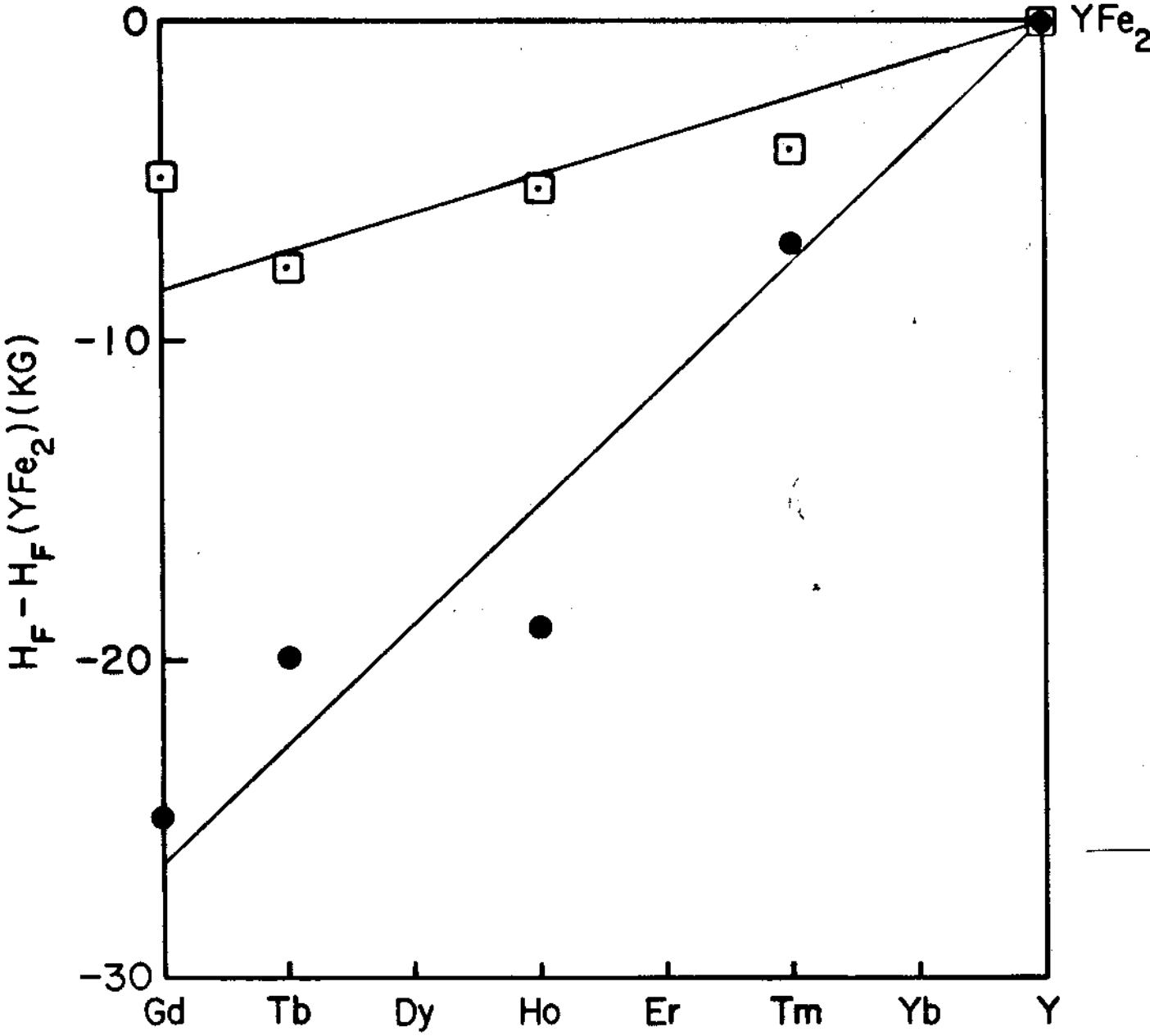

Fig. 6

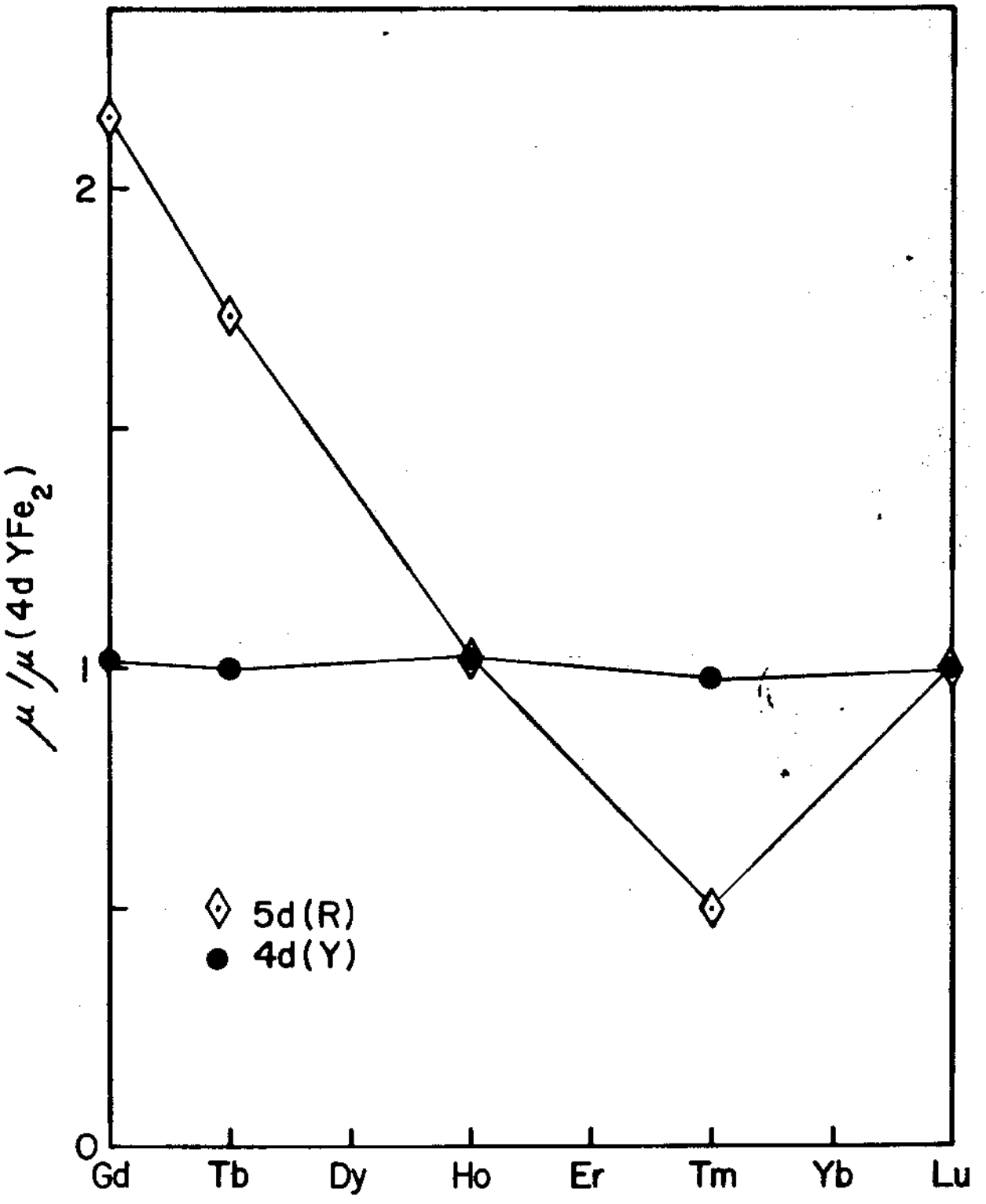

Fig. 7

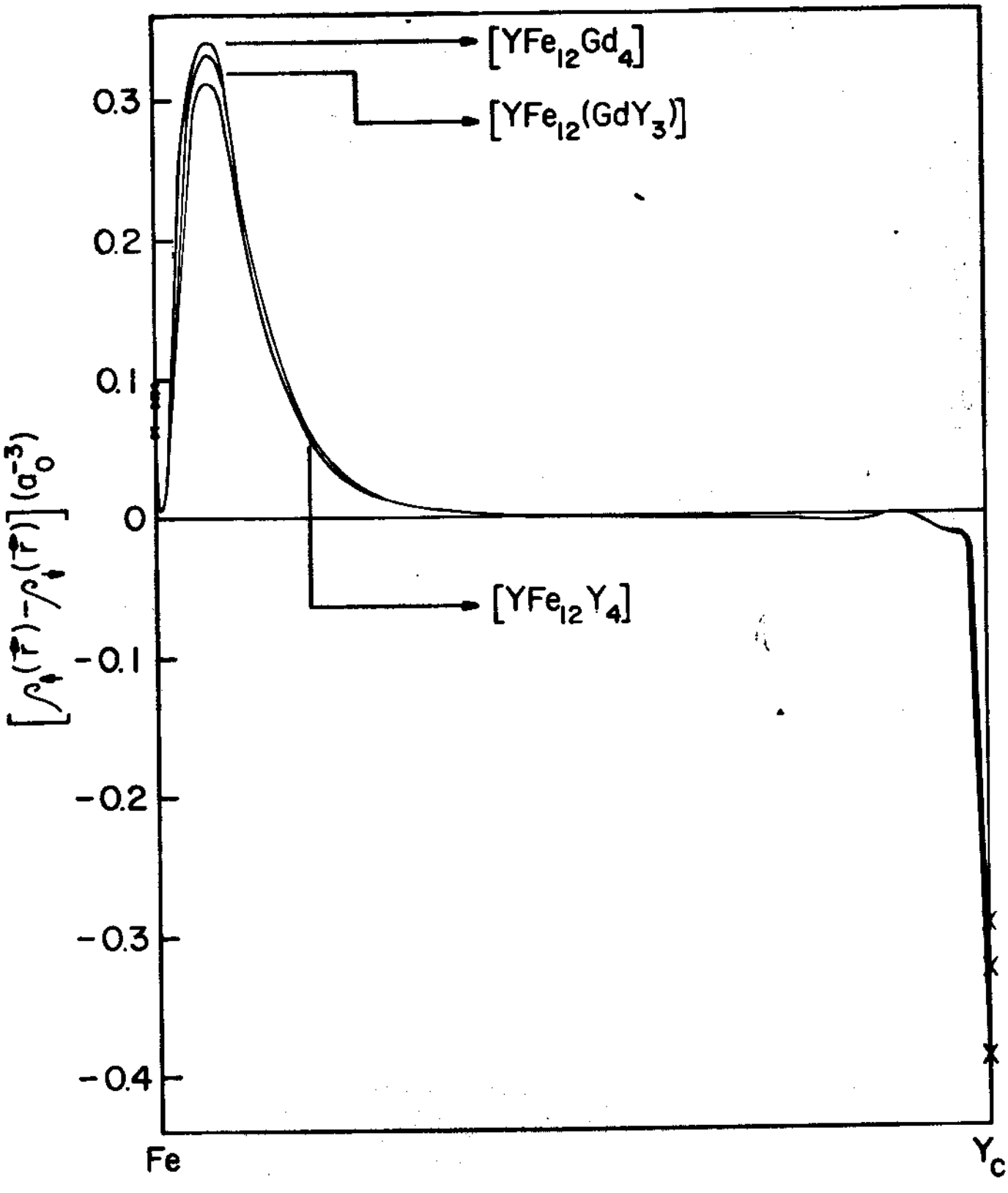
[YFe12Gd4]
[YFe12(GdY3)]
[YFe12Y4]
0.3
0.2
0.1
0
-0.1
-0.2
-0.3
-0.4
[ρ↑(r)-ρ↓(r)] (a0^-3)
Fe
Yc

FIG. 8

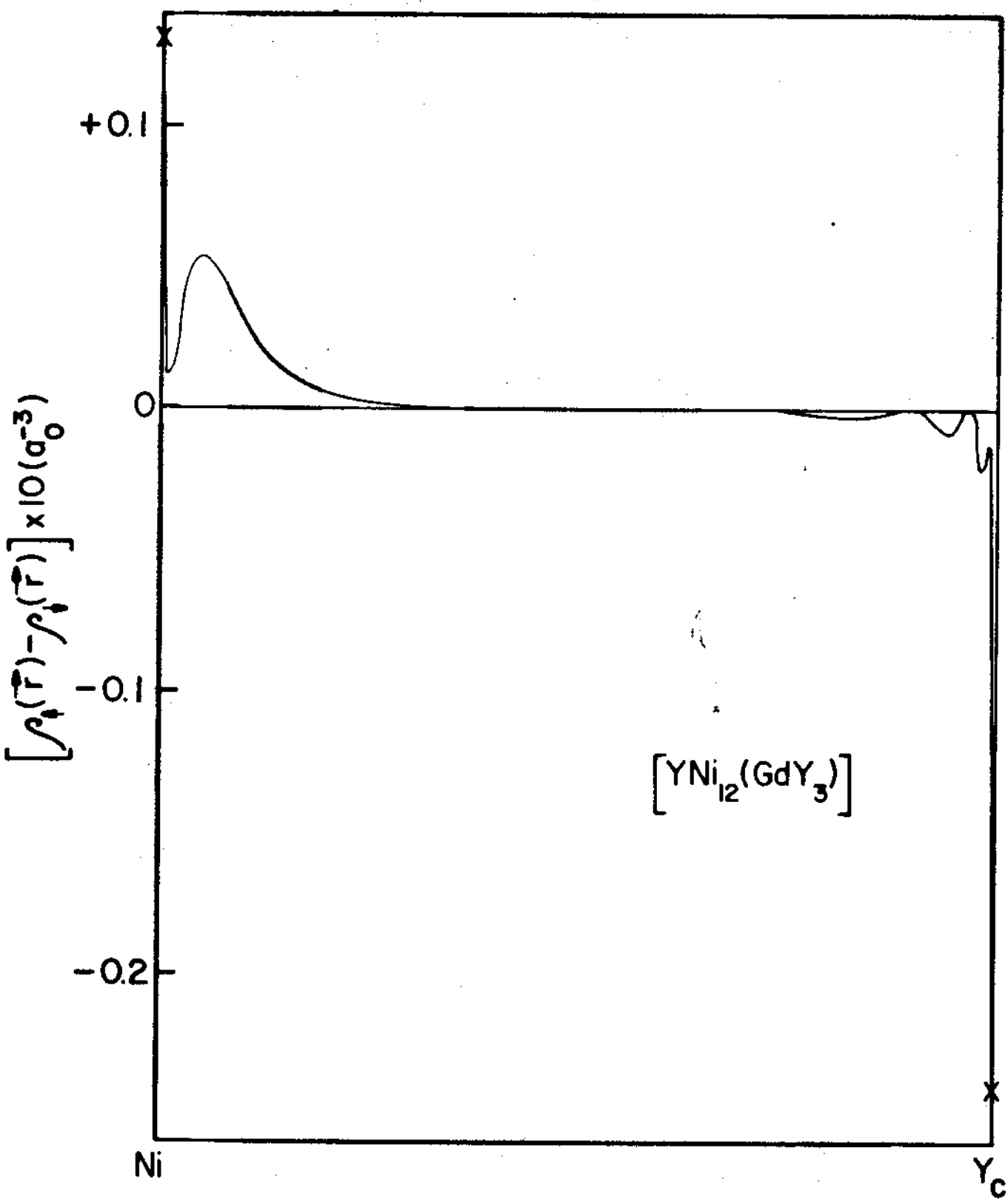
+0.1
0
-0.1
-0.2
$[\rho_\uparrow(\vec{r})-\rho_\downarrow(\vec{r})]\times 10(a_0^{-3})$
$[YNi_{12}(GdY_3)]$
Ni
Y_C

Fig. 9

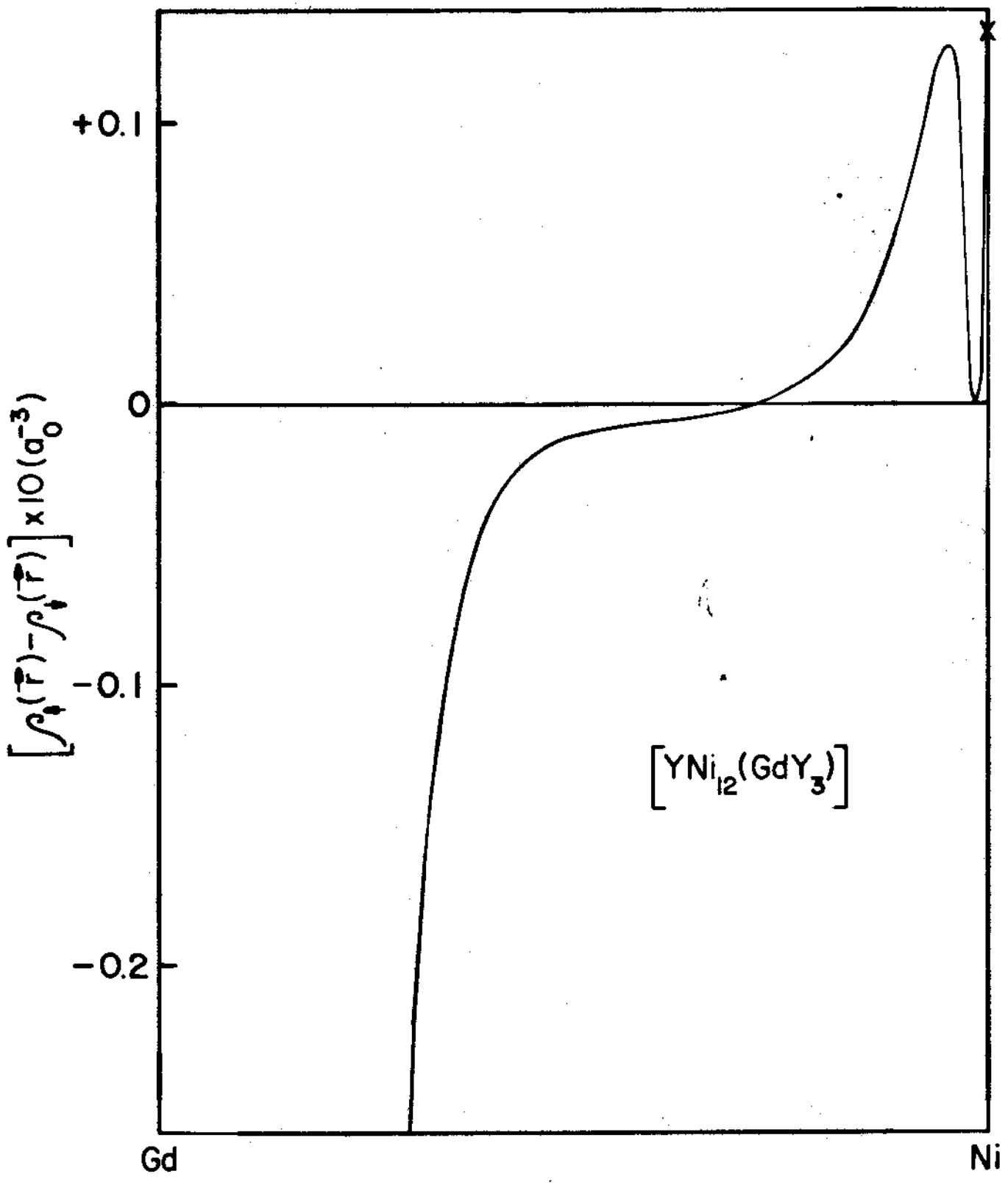
+0.1
0
-0.1
-0.2
$[\rho_\uparrow(\vec{r})-\rho_\downarrow(\vec{r})]\times 10(a_0^{-3})$
$[YNi_{12}(GdY_3)]$
Gd
Ni

Fig. 10

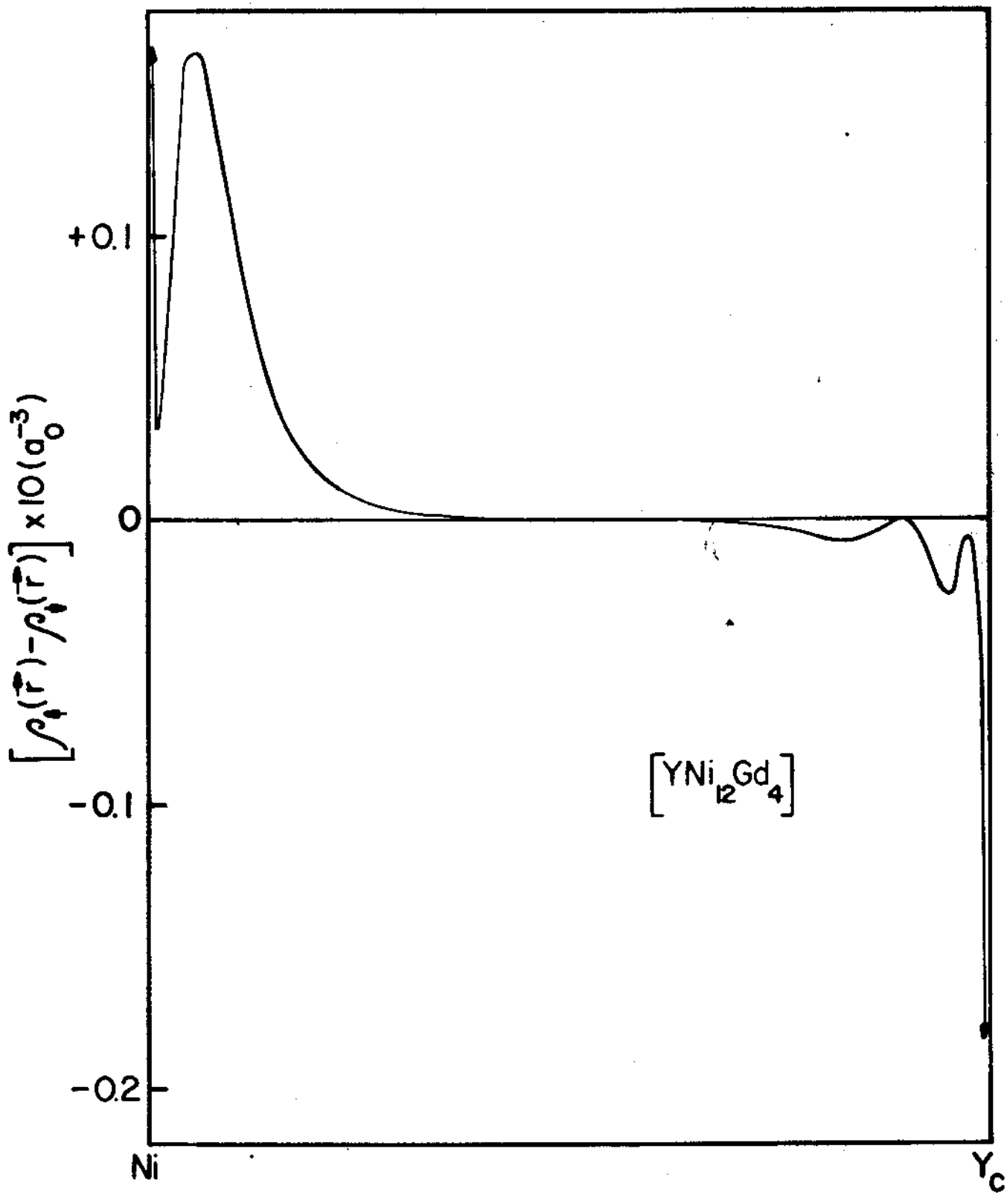
+0.1
0
-0.1
-0.2
$[\rho_\uparrow(\vec{r}) - \rho_\downarrow(\vec{r})] \times 10 (a_0^{-3})$
$[YNi_{12}Gd_4]$
Ni
Y_C

Fig. 11

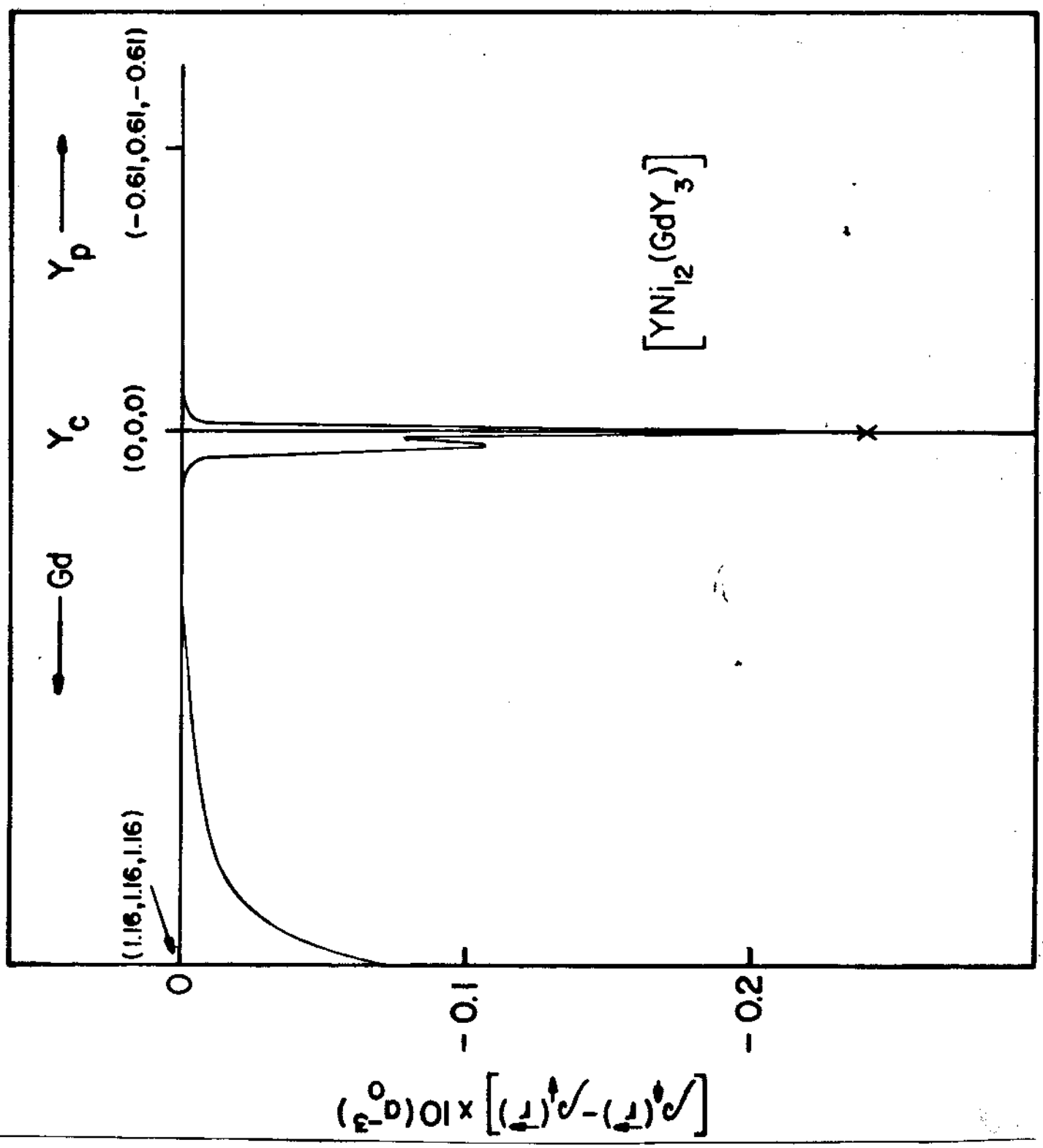
$[YNi_{12}(GdY_3)]$
Y_p
(-0.61,0.61,-0.61)
Y_c
(0,0,0)
Gd
(1.16,1.16,1.16)
0
-0.1
-0.2
$[\rho(T)-\rho(T)] \times 10(\Omega^0_{-3})$

Fig. 12

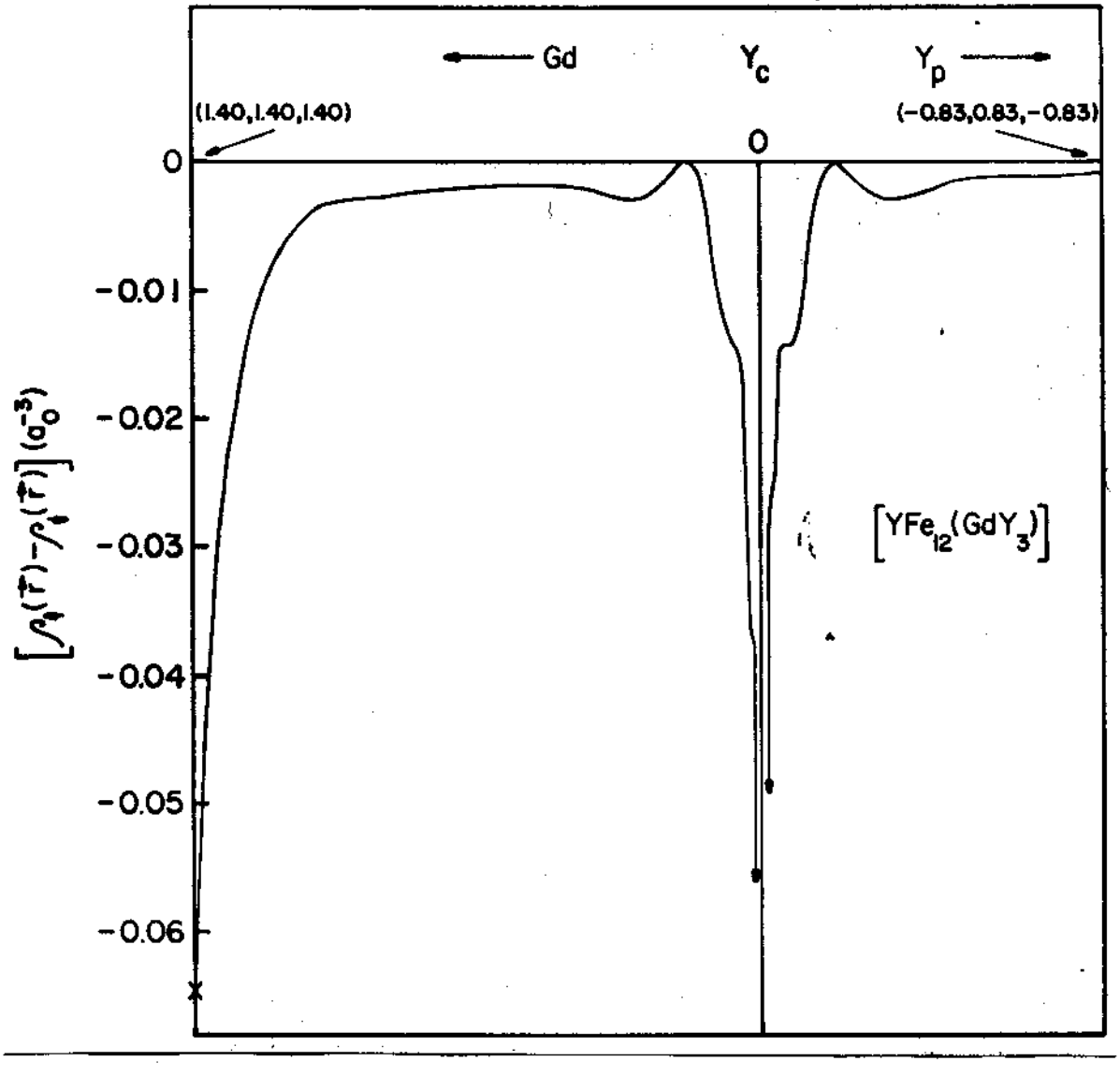
Gd
Y_c
Y_p
(1.40,1.40,1.40)
(-0.83,0.83,-0.83)
0
0
-0.01
-0.02
-0.03
-0.04
-0.05
-0.06
$[\rho_1(\vec{r})-\rho_1(\vec{r})]\,(a_0^{-3})$
$[YFe_{12}(GdY_3)]$

Fig. 13

TABLE I

Compound	Cluster	Charge on Y_c	Charge on Y_p	Charge on R	Charge on Fe	Populations on Y_c	
YFe_2	$[YFe_{12}Y_4]$	+2.0	+2.2	--	-1.1	4d	1.13
						5s	0.04
						5p	0.07
$Y_{1-x}Gd_xFe_2$	$[YFe_{12}(GdY_3)]$	+2.0	+2.2	+1.9	1)-0.8	4d	1.16
					2)-1.6	5s	0.05
					3)-0.9	5p	0.10
	$[YFe_{12}Gd_4]$	+1.9	--	+2.0	-1.0	4d	1.15
						5s	0.04
						5p	0.07
$Y_{1-x}Tb_xFe_2$	$[YFe_{12}(TbY_3)]$	+2.0	+2.2	+1.9	1)-0.8	4d	1.16
					2)-1.6	5s	0.05
					3)-0.9	5p	0.10
	$[YFe_{12}Tb_4]$	+1.9	--	+2.0	-1.0	4d	1.15
						5s	0.05
						5p	0.07
$Y_{1-x}Ho_xFe_2$	$[YFe_{12}(HoY_3)]$	+2.0	+2.2	+2.0	1)-0.8	4d	1.16
					2)-1.6	5s	0.05
					3)-0.9	5p	0.10
	$[YFe_{12}Ho_4]$	+1.9	--	+2.0	-1.0	4d	1.14
						5s	0.05
						5p	0.07
$Y_{1-x}Tm_xFe_2$	$[YFe_{12}(TmY_3)]$	+2.0	+2.2	+1.9	1)-0.8	4d	1.15
					2)-1.6	5s	0.05
					3)-0.9	5p	0.10
	$[YFe_{12}Tm_4]$	+2.0	--	+2.0	-1.0	4d	1.14
						5s	0.04
						5p	0.07
$Y_{1-x}Lu_xFe_2$	$[YFe_{12}(LuY_3)]$	+2.0	+2.2	+2.2	1)-0.8	4d	1.15
					2)-1.7	5s	0.05
					3)-0.9	5p	0.10
	$[YFe_{12}Lu_4]$	+2.0	--	+2.2	-1.1	4d	1.13
						5s	0.04
						5p	0.07

TABLE II

Compound	Cluster	Charge on Y_c	Charge on Y_p	Charge on R	Charge on Fe	Populations on Y_c	
YNi_2	$[YNi_{12}Y_4]$	+1.8	+2.0	--	-1.0	4d	1.30
						5s	0.05
						5p	0.08
$Y_{1-x}Gd_xNi_2$	$[YNi_{12}(GdY_3)]$	+1.9	+2.2	+1.9	1)-0.8	4d	1.24
					2)-1.5	5s	0.05
					3)-1.0	5p	0.13
	$[YNi_{12}Gd_4]$	+1.8	--	+2.0	-1.0	4d	1.24
						5s	0.05
						5p	0.09

TABLE III

Compound	Cluster	μ(4d)	H_D(kG)	H_C(kG)	$H_F \approx H_D + H_C$(kG)
$Y_{1-x}Gd_xNi_2$	$[YNi_{12}(GdY_3)]$	0.00	-6.2	-12.7	-19
	$[YNi_{12}Gd_4]$	-0.01	--	-48.0	-48

REFERENCES

1) Buschow K.H.J. 1977 Rep. Prog. Phys. 40 1179.

2) Ritter C. 1989 J. Phys.:Condens. Matter 1 2765.

3) Armitage J.G.M.,Dumelow T., Riedi P.C. and Abell J.S. 1989 J. Phys.:Condens. Matter 1 3987.

4) Yamada H., Inoue J., Terao K., Kanda S. and Shimizu M. 1984 J. Phys. F: Metal Phys. 14 1943.

5) Mohn P. and Schwarz K. 1985 Physica 130B 26.

6) Eriksson O. and Svane A. 1989 J. Phys.: Condens. Matter 1 1589.

7) Oppelt A. and Buschow K.H.J. 1973 J. Phys. F: Metal Phys. 3 L212.

8) Riedi P.C. and Webber G.D. 1983 J. Phys. F: Metal Physics 13 1057.

9) Alves K.M.B., Alves N., Guimarães A.P., Mackenzie I.S. and Ross J.W. 1986 J. Magn. Magn. Mat. 54-57 501.

10) Ellis D.E. 1968 Int. J. Quant. Chem. S2 35.

11) Ellis D.E. and Painter G.S. 1970 Phys. Rev. B2 2887.

12) Guenzburger D. and Ellis D.E. 1987 Phys. Rev. B36 6971.

13) Guenzburger D., Ellis D.E. and Danon J. 1986 J. Mag. Magn. Mat. 59 139.

14) Chacham H., Galvão da Silva E., Guenzburger D. and Ellis D.E. 1987 Phys. Rev. B35 1602.

15) Guenzburger D. and Ellis D.E. 1991 Phys. Rev. Letters 67 3832.

16) Guenzburger D. and Ellis D.E. 1992 Phys. Rev. B45 285.

17) Guenzburger D. and Ellis D.E. 1985 Phys. Rev. B31 93.

18) Ellis D.E. and Guenzburger D. 1985 Phys. Rev. B31 1514.

19) Alves K.M.B., Alves N., Sampaio L.C., Cunha S.F. and Guimarães A.P. 1990 J. Appl. Phys. 67 5867.

20) Alves K.M.B. and Guimarães A.P. 1991 J. Appl. Phys. 70 7632.

21) Oppelt A. and Buschow K.H.J. 1976 Phys. Rev. B13 4698.

22) Parr R.G. and Yang W. "Density Functional Theory of Atoms and Molecules", Oxford University Press, N. York (1989).

23) Ellis D.E., Benesch G.A. and Byron E. 1977 Phys. Rev. B16 3308.

24) Kohn W. and Sham L.J. 1965 Phys. Rev. 140 A1133.

25) von Barth U. and Hedin L. 1972 J. Phys. C 5 1629.

26) Mulliken R.S. 1949 J. Chem. Phys. 46 479.

27) Delley B. and Ellis D.E. 1982 J. Chem. Phys. 76 1949.

28) Stroud A.H.,"Approximate Calculation of Multiple Integrals", Prentice Hall, Englewood Cliffs (1971).

29) Terra J. and Guenzburger D. 1991 Phys. Rev. B44 8584.

30) Shriver D.F., Atkins P.W. and Lanford C.H., "Inorganic Chemistry", W.H. Freeman, N.York (1990).

31) Buschow K.H.J. and van Stapele R.P. 1970 J. Appl. Phys. 41 4066.

32) Eriksson O., Johansson B., Brooks M.S.S. and Skriver H.L. 1989 Phys. Rev. B40 9519.

33) Guimarães A.P. and Bunbury D.St.P. 1973 J. Phys. F: Met. Phys. 3 885.

34) McCausland M.A.H.and Mackenzie I.S. 1979 Adv. Phys. 28 305.

35) Campbell I.A. 1972 J. Phys.F: Met. Phys. 2 L47.

36) Dumelow T., Riedi P.C., Mohn P., Schwarz K. and Yamada Y. 1986 J. Mag. Magn. Mat. 54-57 1081.